European Cells and Materials Vol.59 2026 (pages 308–326) DOI: 10.22203/eCM.v059a17 ISSN 1473-2262

Original Article

PPAR-α Activators Remodel U87 Cells and Enhance Sunitinib Cytotoxicity via Modulation of Cell Cycle, Apoptosis, *TAOKs*/*Cadherins* Gene Expression and Histone Demethylase

Saad Alobid[1], Muhannad Alqahtani[1], Hussam Albassam[1], Faris Almutairi[1], Mohammed M. Alanazi[2], Ahmed H. Bakheit[2], Hanadi H. Asiri[2] and Gamaleldin I. Harisa[3,*]

[1]Department of Pharmacology and Toxicology, College of Pharmacy, King Saud University, 11451 Riyadh, Saudi Arabia
[2]Department of Pharmaceutical Chemistry, College of Pharmacy, King Saud University, 11451 Riyadh, Saudi Arabia
[3]Department of Pharmaceutics, College of Pharmacy, King Saud University, 11451 Riyadh, Saudi Arabia

Abstract

Background: Glioblastoma multiforme (GBM) is an aggressive and highly invasive primary brain tumor characterized by poor clinical outcomes and limited therapeutic options, emphasizing the need for novel treatment strategies. Fenofibrate (FEN), a peroxisome proliferator-activated receptor alpha (PPAR-α) agonist widely used for dyslipidemia, has demonstrated anticancer effects through the modulation of cellular proliferation, apoptosis, and metabolic pathways. This study explored the therapeutic potential of FEN alone and in combination with sunitinib (SNB) against U87 glioblastoma (GB) cells. **Methods**: U87 cells were treated with FEN, SNB, or their combination. Cell viability, apoptosis, and cell-cycle progression were evaluated. The expression of tumor protein 53 (*TP53*), BCL2 associated X, apoptosis regulator (*BAX*), epithelial cadherin (*CDH1*), neural cadherin (*CDH2*), thousand and one kinase 1 (*TAOK1*), and thousand and one kinase 2 (*TAOK2*) was assessed using quantitative reverse transcription polymerase chain reaction (RT-PCR). Molecular docking was performed to examine the potential interactions of fenofibric acid (FFA) and SNB with GBM-related molecular targets. **Results**: FEN and SNB reduced U87 cell viability in a dose-dependent manner, while combined treatment produced greater cytotoxicity than either agent alone. The combination induced the highest level of apoptosis and enhanced G1-phase cell-cycle arrest. Treatment also increased *TP53*, *BAX*, and *CDH1* expression while decreasing *CDH2*, *TAOK1*, and *TAOK2* expression. Molecular docking demonstrated favorable interactions of FFA and SNB with multiple targets implicated in GBM progression. **Conclusions**: FEN combined with SNB exhibited enhanced anticancer activity against U87 GB cells through induction of apoptosis, cell-cycle arrest, and modulation of tumor-related genes. These findings support the potential of FEN/SNB combination therapy as a promising therapeutic strategy for GBM and provide a basis for further preclinical investigation.

Keywords: Fenofibric acid, drug repurposing, *TAOK* kinases, DNA methyltransferases, sialyltransferase, cyclin-dependent kinase 4.

***Address for correspondence**: Gamaleldin I. Harisa, Department of Pharmaceutics, College of Pharmacy, King Saud University, 11451 Riyadh, Saudi Arabia. E-mail: harisa@ksu.edu.sa.

Copyright policy: © 2026 The Author(s). Published by Forum Multimedia Publishing, LLC. This article is distributed in accordance with Creative Commons Attribution Licence (http://creativecommons.org/licenses/by/4.0/).

Introduction

Malignant transformation is characterized by the interruption of usual cellular programming at metabolic, genetic, and epigenetic levels, leading to aberrant signaling pathways and increased uptake of glucose, fatty acids, and amino acids to support tumor growth [1]. Tumorigenesis is driven by mutations that disturb the equilibrium between oncogenes and tumor suppressor genes. Moreover, epigenetic changes such as DNA methylation and histone modifications that silence tumor suppressor genes or activate proto-oncogenes [1]. Additionally, diminishing of programmed cell death (PCD), including apoptosis and ferroptosis, facilitates oncogenesis [2]. Cancer cells also display imbalance of sialyltransferase (SIT)/sialidase expression, resulting in membrane hypersialylation that promotes proliferation, invasion, metastasis, immune escaping, and therapeutic resistance [3,4]. These molecular changes contribute to the development of numerous malignancies, including breast, lung, liver, and glioblastoma multiforme (GBM) [1,5].

GBM is the most aggressive primary brain tumor and is associated with rapid progression, marked heterogeneity, and poor prognosis despite advances in multimodal therapy [6–8]. Risk factors, including aging, genetic predisposition, obesity, inflammation, head injury, smoking, alcohol con-

sumption, radiation, nitrosamines, and other environmental xenobiotics, contribute to malignant transformation at genetic and epigenetic alterations in glial cells [6–8]. Molecularly, GBM growth is driven by dysregulation of oncogenic and tumor suppressor pathways. Isocitrate dehydrogenase (IDH)-wildtype tumors commonly harbor epidermal growth factor receptor (EGFR) amplification and mutations in tumor protein 53 (*TP53*), neurofibromin-1, and phosphatase and tensin homolog, whereas IDH-mutant tumors frequently exhibit platelet-derived growth factor receptor alpha modifications and additional tumor suppressor gene mutations [9]. Epigenetic modifications further contribute to GBM heterogeneity and disease progression [8]. GBM cells undergo profound metabolic remodeling to sustain rapid proliferation, including enhanced glucose utilization, lipid metabolism, and glutamine dependency [5,6]. Their reliance on aerobic glycolysis increases methylglyoxal (MGO) production [10], while altered SIT and sialidase expression promotes hypersialylation and formation of a protective glycan coat on the cell surface [11]. These changes enhance tumor aggressiveness, invasion, immune escape, and drug resistance, highlighting metabolic and glycosylation pathways as attractive therapeutic targets [10, 11].

Present GBM management relies on maximal surgical resection followed by radiotherapy and chemotherapy; however, therapeutic efficacy remains limited because of extensive tumor heterogeneity, infiltrative growth, blood-brain barrier (BBB) constraints, and treatment resistance [6,12,13]. Consequently, combination therapy and drug repurposing have emerged as promising strategies to improve clinical outcomes [14–16]. Several approved drugs, including antidiabetic, antimicrobial, anti-inflammatory, antihistamine, cannabinoid, hormone-modulating, and lipid-lowering agents, have demonstrated potential anticancer activity and are being examined for GBM treatment [15–17]. Among repurposed agents, lipid-lowering drugs have attracted considerable interest because of their pleiotropic anticancer effects [17–19]. Fenofibrate (FEN), a peroxisome proliferator-activated receptor alpha (*PPAR-*α) agonist, inhibits tumor cell proliferation, migration, angiogenesis, and survival while exhibiting relatively low systemic toxicity [19–22]. Experimental evidence suggests that FEN induces apoptosis in GBM cells and may promote phenotypic restoration of malignant cells [21,22]. Sunitinib (SNB), a multi-targeted tyrosine kinase inhibitor (TKI), suppresses receptor tyrosine kinase signaling by competitively inhibiting ATP binding and downstream proliferative pathways [14,23]. Nevertheless, its therapeutic efficacy in GBM is limited by tumor heterogeneity, poor BBB penetration, off-target effects, and the requirement for relatively high doses [14]. Therefore, combining FEN with SNB may simultaneously target complementary molecular pathways and enhance therapeutic efficacy.

Restoring malignant cells toward a less aggressive phenotype has emerged as an innovative therapeutic strategy [24–26]. Rather than solely inducing cytotoxicity, cancer cell remodeling aims to reverse malignant characteristics by restoring normal cellular functions and regulatory networks [25,26]. Small molecules, biologics, and approaches targeting cancer stem cells have shown promise in promoting phenotypic restoration [24–26]. Moreover, computational-based drug discovery is facilitating the identification of compounds capable of modulating these reprogramming pathways [27].

Together, these advances support cancer cell remodeling as a complementary therapeutic paradigm for improving treatment responsiveness. Therefore, this study aims to explore the effects of FEN, alone and in combination with SNB, on glioblastoma (GB) cell viability and phenotypic remodeling using U87 cells as an *in vitro* GBM model. Cell viability, cell cycle progression, apoptosis, and the expression of oncogenic markers (thousand and one kinase 1 (*TAOK1*), thousand and one kinase 2 (*TAOK2*), and epithelial cadherin (*CDH1*)) and tumor suppressor genes (*TP53*, BCL2 associated X, apoptosis regulator (*BAX*), and neural cadherin (*CDH2*)) were evaluated using 3-(4,5-dimethylthiazol-2-yl)-2,5-diphenyltetrazolium bromide (MTT) assay, flow cytometry, and quantitative reverse transcription polymerase chain reaction (RT-PCR). In addition, molecular docking was performed to predict the interactions of FEN and SNB with molecular targets implicated in GBM phenotypic restoration, including DNA methyltransferase (DNMT), histone demethylase (HDM), α-ketoglutarate dehydrogenase (KGDH), isocitrate dehydrogenase-2 (IDH2), succinate dehydrogenase (SDH), SIT, glyoxalase-1 (GLO-1), cyclin-dependent kinase 4 (CDK4), Caspase-8, and glutathione peroxidase-4 (GPX4).

Materials and Methods

Materials

FEN (49562-28-9) and SNB (557795-19-4) were purchased from Sigma-Aldrich (St. Louis, MO, USA). All other reagents of the highest commercial grade, unless indicated, were obtained from Sigma Chemical Co. (St. Louis, MO, USA).

Cell Mortality Studies

Human GB astrocytic U87 cells (HTB-14) were obtained from ATCC (Manassas, VA, USA) and authenticated by Short Tandem Repeat (STR) profiling to ensure identity and genetic stability. Cells were cultured in Dulbecco's Modified Eagle's Medium (DMEM, 21063029; Gibco, Grand Island, NY, USA; 1×; Gibco®) supplemented with 10% fetal bovine serum (FBS, 11I249; VivaCell, Shanghai, China) and 1% penicillin–streptomycin (15140148; Thermo Fisher Scientific, Waltham, MA, USA), and maintained at 37 °C in a humidified incubator (BZTHI-502, Labzee, Crawley, United Kingdom) with 5% CO_2. Stan-

dard sterile techniques, including the use of a laminar flow hood (Heraguard ECO, Thermo Fisher Scientific, Waltham, MA, USA) and routine mycoplasma testing, were applied to preserve culture integrity. Subculturing was performed at 85–90% confluence, and cells from passages 5–20 with 80–90% confluence were used for experiments.

Cell viability was evaluated using the MTT assay. U87 cells were seeded in 96-well plates at a density of 2.5×10^4 cells per well in 100 μL of medium. The cells were treated with 1% dimethyl sulfoxide (DMSO, 276855; Sigma-Aldrich, St. Louis, MO, USA) for control, SNB, FEN, or their combination. The doses of SNB and FEN were selected depending on the previously published work [28,29]. After 24 hours treatment FEN, SNB, or their combination, 10 μL of MTT (M2128; Sigma-Aldrich, St. Louis, MO, USA) solution (5 mg/mL) was added to each well and incubated for 3 hours at 37 °C. The medium was removed, formazan crystals were dissolved in 100 μL DMSO, and absorbance was measured at 570 nm using a BioTek ELx-800 microplate reader (BioTek Instruments, Inc., Winooski, VT, USA).

Apoptosis Assay

U87 cells were seeded under appropriate culture conditions, allowed to adhere overnight, and treated for 24 hours with FEN (150 μM), SNB (100 nM), or their combination (FEN 150 μM + SNB 100 nM). U87 cells were then collected, washed twice with 1× phosphate buffer saline (PBS), and stained with Annexin V-FITC (640932; BioLegend, CA, USA) and propidium iodide (P4170; Sigma-Aldrich, St. Louis, MO, USA) according to the MedChemExpress procedure. Apoptosis and necrosis percent were measured using a Beckman Coulter FC500 flow cytometer, catalog no. 626553, with MXP Software (Beckman Coulter, Inc., Brea, CA, USA), permitting differentiation between viable, early apoptotic, and late apoptotic or necrotic cells.

Cell Cycle Assay

U87 cells were plated in 6-well plates, allowed to adhere overnight, then treated for 24 hours with FEN (150 μM), SNB (100 nM), or their combination (FEN 150 μM + SNB 100 nM). After treatment, cells were trypsinized, washed twice with PBS, fixed in 70% cold ethanol, and incubated for 12 h. Fixed cells were centrifuged, resuspended in 500 μL propidium iodide (10 μg/mL) with Ribonuclease (RNase) (300 μg/mL), and incubated on ice for 30 min. DNA content of 10,000 cells per sample was measured on a FACSCalibur flow cytometer (FC500 Flow Cytometer), and cell-cycle distributions (G1, S, G2/M) were analyzed with ModFit LT® (Verity Software House, Topsham, ME, USA).

Table 1. The mRNA primer sequences for the *TP53*, *BAX*, *CDH1*, *CDH2*, *TAOK1*, and *TAOK2* genes, along with *GAPDH* as housekeeping gene.

Genes	The mRNA primer sequences
TP53	F: 5′ TCAGCATCTTATCCGAGTGGAA 3′
	R: 5′ AGGGCACCACCACACTATGTC 3′
BAX	F: 5′ GTCTCCGGCGAATTGGAGAT 3′
	R: 5′ ACCCGGAAGAAGACCTCTCG 3′
CDH1	F: 5′ CCTCCAGAGTTTACTGCCATGAC 3′
	R: 5′ GTAGGATCTCCGCCACTGATTC 3′
CDH2	F: 5′ GAACAGCACGTACACAGCCCT 3′
	R: 5′ GCAGAACTGTCCCTGTCCCAG 3′
TAOK1	F: 5′ GGCGTCATAACTTAGAGCAGGAC 3′
	R: 5′ TTGTGTTGAGGTGGCGGAACTC 3′
TAOK2	F: 5′ TGTCGCCAGTACAAGCGCAAGA 3′
	R: 5′ GCACACTCCAAGTCCTTCTGG 3′
GAPDH	F: 5′ CGTGGAAGGATCCATGACCA 3′
	R: 5′ GCCATCACGCCACAGTTTC 3′

Gene Expression Studies

U87 cells were treated for 24 hours with FEN (150 μM), SNB (100 nM), or their combination (FEN 150 μM + SNB 100 nM), then total RNA was extracted using TRIzol (15596026; Thermo Fisher Scientific, Waltham, MA, USA) per the manufacturer's instructions. RNA levels were assessed using NanoDrop Ultra (μg/μL; Thermo Fisher Scientific, Waltham, MA, USA), and cDNA was synthesized with the SuperScript VILO kit (Thermo Scientific, Wilmington, DE, USA). Quantitative RT-PCR for *TP53*, *BAX*, *CDH1*, *CDH2*, *TAOK1*, and *TAOK2* was performed using TaqMan Gene Expression Master Mix (4369016; Applied Biosystems, Thermo Fisher Scientific, Waltham, MA, USA) on a Rotor-Gene Q (QIAGEN, Hilden, Germany). Glyceraldehyde-3-phosphate dehydrogenase (*GAPDH*) served as the reference housekeeping gene. Thermal cycling: 50 °C for 2 min, 95 °C for 10 min, then 40 cycles of 95 °C for 15 s and 60 °C for 1 min. Table 1 presents the primer sequences of *TP53*, *BAX*, *CDH1*, *CDH2*, *TAOK1*, *TAOK2* and *GAPDH* genes.

Molecular Docking Studies

FEN is a prodrug that undergoes hydrolysis by esterases to produce fenofibric acid (FFA), which is the biologically active form responsible for *PPAR-α* activation and most of the pharmacological effects observed *in vivo*. Therefore, FFA was selected for the molecular docking studies because it represents the active molecular species that directly interacts with protein targets.

Non-covalent docking was performed using the Molecular Operating Environment (MOE) software (Chemical Computing Group ULC, Montreal, Quebec, Canada) suite, MOE version 2024.10, to evaluate the binding interactions of SNB and FFA with the selected molecular targets listed in Table 2. Ligands were prepared

by energy minimization, partial charge assignment, and protonation at pH 7.4 using the Protonate 3D method, then saved in Molecular Database (MDB) format. Protein targets were similarly prepared by hydrogen addition, receptor refinement, protonation using Protonate 3D, partial charge assignment using the AMBER10:EHT force field, and energy minimization. Binding sites were defined from co-crystallized ligand coordinates when available, or from the reported catalytic/binding pocket. Docking was performed using the same validated protocol; ligand placement was carried out using the Triangle Matcher method, preliminary scoring was performed using London dG, and final poses were rescored using Generalized Born Volume Integral/Weighted Surface Area free energy of binding (GBVI/WSA) dG. The best poses were selected based on docking score, correct occupation of the binding pocket, absence of severe steric clashes, hydrogen bonding distance $\leq$3.5 Å, and the presence of stabilizing interactions, including hydrophobic, aromatic, electrostatic, and metal-coordination interactions when applicable.

Irreversible covalent docking of SNB with GPX4 and Caspase-8 was performed using the covalent docking module of MOE software suite, version 2024.10. The protein targets were prepared by hydrogen addition, protonation, AMBER10:EHT partial charge assignment, and energy minimization. The reactive cysteine residues, reactive cysteine residues (Cys66) in GPX4 and Cys285 in Caspase-8, were predefined as nucleophilic reaction sites, while the electrophilic Michael-acceptor region of SNB was assigned as the reactive ligand site. Covalent docking was modeled through a Michael addition reaction between the cysteine thiol/thiolate sulfur and SNB, resulting in C–S covalent bond formation. The best poses were selected based on successful covalent bond formation, proper orientation within the hydrophobic pocket, favorable docking score, absence of steric clashes, and stabilizing non-covalent interactions. These covalent docking results were considered computational predictions requiring experimental validation.

Table 2. Selected biological targets for molecular docking workflow.

Targets	Code	PDB
Caspase-8	CAS-8	1QDU
Glutathione peroxidase-4	GPX4	7U4K
DNA methyltransferase	DNMT	4DA4
Histone demethylase	HDM	4ASK
Sialyltransferase	SIT	4JS2
Glyoxalase I	GLO-1	9KEE
Isocitrate dehydrogenase-2	IDH2	5L57
α-ketoglutarate dehydrogenase	KGDH	7WGR
Succinate dehydrogenase	SDH	2FBW
Cyclin-dependent kinase-4	CDK4	7SJ3

Statistical Analyses

The data of this study were analyzed using GraphPad InStat software, version 5 (GraphPad Software, Inc., La Jolla, CA, USA). A one-way analysis of variance was used to relate the results. Data are displayed as mean ± standard deviation (SD). *p*-value of $\leq$0.05 was used as the criterion for statistical significance. The images were drawn with GraphPad Prism (version 5; GraphPad Software, Inc., La Jolla, CA, USA).

Results

Impact of SNB and FEN and Their Combination on U87 Mortality

In the present study, untreated U87 cells showed 100% viability, serving as a reference control group. In the SNB treatment group, SNB induces a stronger increase in cell death than FEN at comparable concentrations, consistent with its known anti-tumor activity. Viability was significantly reduced, indicating potent growth-inhibitory effects. See Fig. 1**A**.

In the FEN-treated group, FEN encouraged U87 cell death in a concentration-dependent manner. Low concentrations cause a modest decline in viability compared with control, whereas higher concentrations lead to a noticeable and progressive reduction of cell growth, reaching roughly 50–60% viability at the highest doses. This indicates a dose-dependent cytotoxic effect of FEN. See Fig. 1**B**. In combined FEN plus SNB treatment, there was the greatest increase in U87 cell mortality compared with either agent alone. U87 cells' survival was significantly lower than that of control and lower than single FEN or SNB treatments, suggesting enhanced inhibitory effect on U87 cell survival. See Fig. 1**C**.

Impact of SNB and FEN and Their Combination on U87 Cells Apoptosis

Annexin V-FITC/PI flow-cytometric analysis was used to assess apoptosis and necrosis in U87 cells after 24 h of treatment with (**A**) control, (**B**) FEN, (**C**) SNB, and (**D**) the SNB + FEN combination (Fig. 2). The majority of cells remained in the viable quadrant (Annexin V^-/PI^-; AP3), representing 97.7% in the control, 96.9% with FEN, 97.3% with SNB, and 95.8% with SNB + FEN. Early apoptotic cells (Annexin V^+/PI^-; AP4) accounted for 1.6%, 1.3%, 0.2%, and 0.2%, respectively, while late apoptotic/necrotic cells (Annexin V^+/PI^+; AP2) represented 0.2%, 0.3%, 0.1%, and 0.1%, respectively.

Overall, the apoptotic populations remained low, and no statistically significant differences were observed among the treatment groups compared with the control at 24 h. These findings suggest that the treatments did not produce a significant phenotypic apoptotic response at this time point. However, a 24-h assessment alone may not be sufficient to capture the full progression of apoptosis, as molecular changes associated with apoptotic signaling may precede

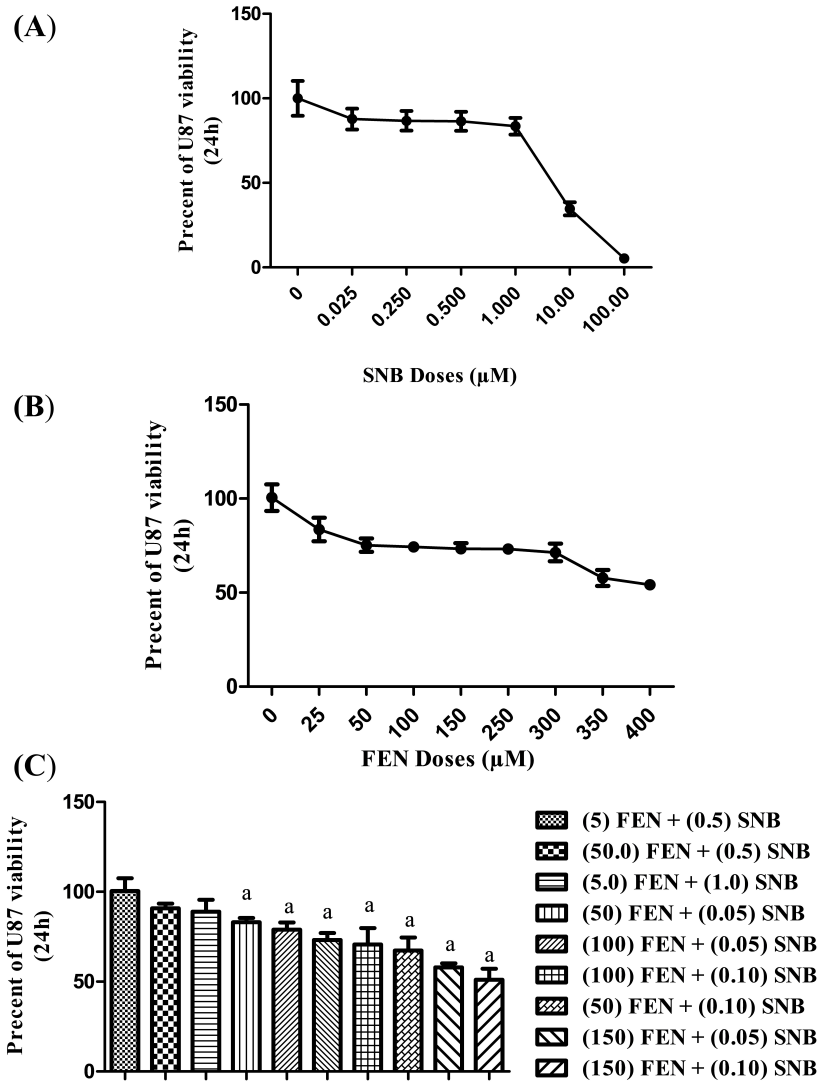


Fig. 1. Effect of sunitinib (SNB), fenofibrate (FEN), and their combination (FEN + SNB) on the viability of U87 GB cells after 24 h of treatment, relative to untreated control cells. (**A**) Effect of SNB. (**B**) Effect of FEN. (**C**) Effect of combined FEN and SNB treatment. Data are presented as the mean ± SD (n = 3). The letter (a) indicate statistically significant differences compared with the control group ($p \leq 0.05$).

the appearance of detectable Annexin V/PI-positive cells.

Therefore, longer and multiple time-point analyses may be required to determine whether the observed treatment-induced molecular changes subsequently translate into a more pronounced apoptotic phenotype.

Impact of SNB and FEN and Their Combination on the U87 Cell-Cycle Program

In the present study, the influence of FEN, SNB, and their combination on cell cycle progression in U87 GB cells was evaluated by flow cytometry, see Fig. 3. The control group in panel (**A**) demonstrated a normal cell cycle distribution, with the majority of cells residing in the G0/G1 phase and smaller proportions in the S and G2/M phases. Treatment with FEN in panel (**B**) caused in a noticeable change in cell cycle distribution, characterized by an accumulation of cells in the G0/G1 phase, suggesting cell cycle arrest at this checkpoint. In contrast, SNB treatment (**C**) induced a marked increase in cell population in the G2/M phase, indicating arrest at the G2/M transition.

Importantly, the combination treatment (SNB + FEN) (**D**) exhibited the most significant effect on cell cycle progression, with a considerable increase in cell accumulation at both G0/G1 and G2/M phases, accompanied by a reduction in the S phase population. This pattern indicates enhanced inhibition of cell cycle progression and DNA synthesis.

The quantitative cell-cycle analysis shows that SNB alone produced only a modest alteration in cell-cycle distribution compared with the control group. In contrast, FEN

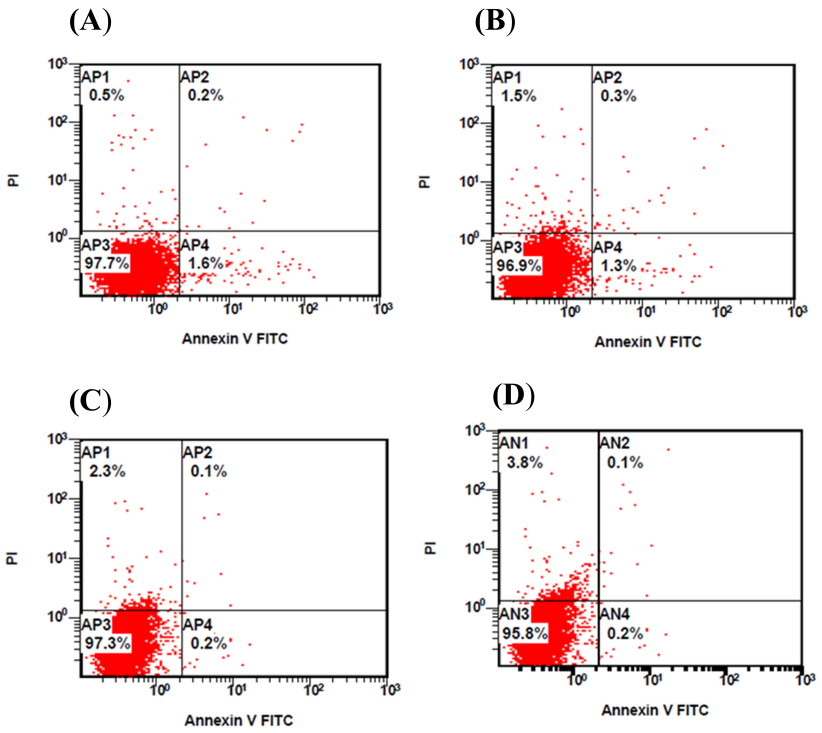


Fig. 2. Effects of sunitinib (SNB), fenofibrate (FEN), and their combination (SNB + FEN) on apoptosis and necrosis in U87 cells, assessed using Annexin V-FITC/PI flow cytometry after 24 h of treatment. (**A**) Control, (**B**) FEN, (**C**) SNB, and (**D**) SNB + FEN.

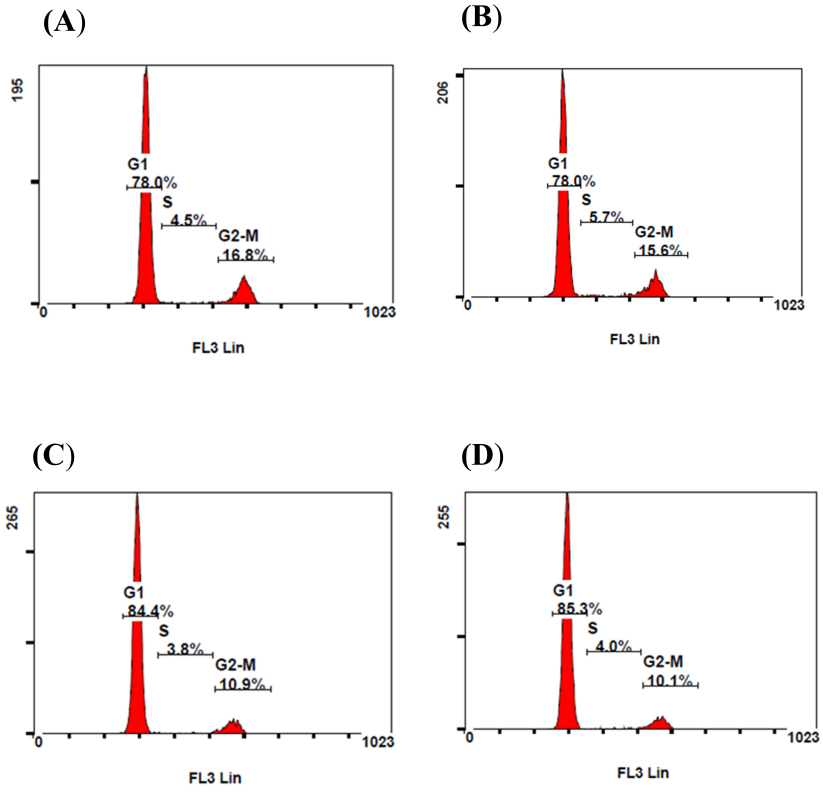


Fig. 3. Effect of sunitinib (SNB), fenofibrate (FEN), and their combination (SNB + FEN) on U 87 cell-cycle program versus control. (**A**) Control, (**B**) FEN, (**C**) SNB, (**D**) SNB + FEN.

markedly increased the proportion of cells in the G0/G1 phase, from 78.02% in the control group to 84.43%, accompanied by a reduction in the G2/M population from 16.78% to 10.93%. The combination treatment produced the highest G0/G1 population (85.25%) and the lowest G2/M population (10.07%). These findings support a treatment-induced accumulation of cells in the G0/G1 phase, particularly following FEN and combination treatment. Collectively, these findings suggest that FEN and SNB differentially modulate cell cycle checkpoints, while their combination exerts a stronger inhibitory effect on U87 cell proliferation.

Impact of SNB and FEN and Their Combination on TP53 and BAX Genes

In the current study, Fig. 4 shows the effects of SNB, FEN, and their combination on the expression of *TP53* gene expression (**A**), *BAX* (**B**), and *CDH1* (**C**) in U87 cells after 24 hours, with each treatment compared to the untreated control group. In Fig. 4**A** *TP53* gene expression, treatment with SNB alone caused in a statistically significant increase in *TP53* gene expression versus the control group, indicating that SNB independently modulates tumor suppressor signaling. Similarly, FEN treatment caused a significant increase in *TP53* expression compared to control cells, indicating its direct impact on U87 cell apoptosis. Importantly, the combined treatment (SNB + FEN) also showed a statistically significant increase compared with the control, suggesting that the dual therapy exerts a strong regulatory effect on *TP53* expression. The changes in *TP53* gene expression governs cell cycle arrest, DNA repair, and apoptosis, suggest treatment-induced modulation of cellular stress and survival pathways.

The expression of *BAX*, a pro-apoptotic gene that promotes mitochondrial-mediated apoptosis, indicates whether the treatments enhance PCD mechanisms. In Fig. 4**B** (*BAX* gene expression), SNB-treated cells exhibited a significant increase in BAX expression compared with the control group. As well, FEN treatment significantly enhances *BAX* expression compared with control cells. The combination treatment showed a statistically significant increase compared with the control group, suggesting an enhanced modulation of apoptosis-related gene expression relative to untreated cells. However, the dual therapy exerts a strong regulatory effect on *TP53* expression when compared with untreated cells.

Impact of SNB and FEN and Their Combination on CDH1 *and* CDH2 *Gene Expression*

In the present results, Fig. 4**C** (*CDH1* gene expression), revealed that SNB treatment alone significantly enhanced *CDH1* expression compared with control cells. Likewise, FEN treatment also resulted in a statistically significant increase relative to the control. SNB plus FEN treatment produced a marked increase compared with the control group. This reflects a pronounced effect of combined FEN and SNB therapy on adhesion-related gene expression relative to untreated conditions. The significant change of *CDH1* expression in treated cells compared with control cells implies an effect on cell–cell adhesion properties. *CDH1* is an epithelial adhesion molecule whose upregulation is generally associated with reduced invasiveness and suppression of epithelial-mesenchymal transition (EMT).

CDH2 expression, a mesenchymal marker often associated with enhanced cell migration, invasiveness, and tumor progression, changes in its expression reflect potential modulation of EMT-related behavior. In Fig. 5**A** (*CDH2*), SNB treatment resulted in a statistically significant decrease in *CDH2* expression compared with control cells. Similarly, FEN-treated cells also showed a significant decrease in *CDH2* expression relative to the control group. The combined SNB plus FEN treatment significantly decreases *CDH2* level compared to control.

Impact of SNB and FEN and Their Combination on TAOK Genes

TAOK1 and *TAOK2* genes encode thousand-and-one amino acid kinases that play important roles in stress response signaling, cytoskeletal regulation, and mitogen-activated protein kinase (MAPK) pathway activation. Variations in the *TAOK* gene expression may influence intracellular signaling networks linked to cell survival and adaptation to stress. In the current study, SNB alone caused a statistically significant decrease in *TAOK1* expression when compared with the control group, reflecting modulation of stress-activated kinase signaling (Fig. 5**B**). FEN treatment also produced a significant decrease relative to control cells, confirming its effect on intracellular signaling pathways. The combined treatment significantly decreased *TAOK1* gene expression compared to controls, suggesting a more substantial disruption of *TAOK1*-related signaling compared with baseline conditions. Fig. 5**C** displays *TAOK2* gene expression; SNB-treated cells showed a significant decrease in *TAOK2* expression compared to the control group. Similarly, FEN treatment resulted in a statistically significant decrease relative to control cells. The combination of SNB and FEN also significantly decreases *TAOK2* expression compared with the control.

Interaction of SNB and FFA With DNMT, HDM, IDH2, and CDK4

Docking analysis shows that both FFA and SNB bind to the DNMT catalytic pocket, but SNB exhibits stronger affinity and more optimal positioning, with a docking score of –8.242 kcal/mol compared with –6.838 kcal/mol for FFA. FFA forms peripheral hydrogen bond interactions with SAM-binding residues, suggesting weaker engagement. In contrast, SNB establishes key interactions within the active site, enhancing stability and inhibitory potential.

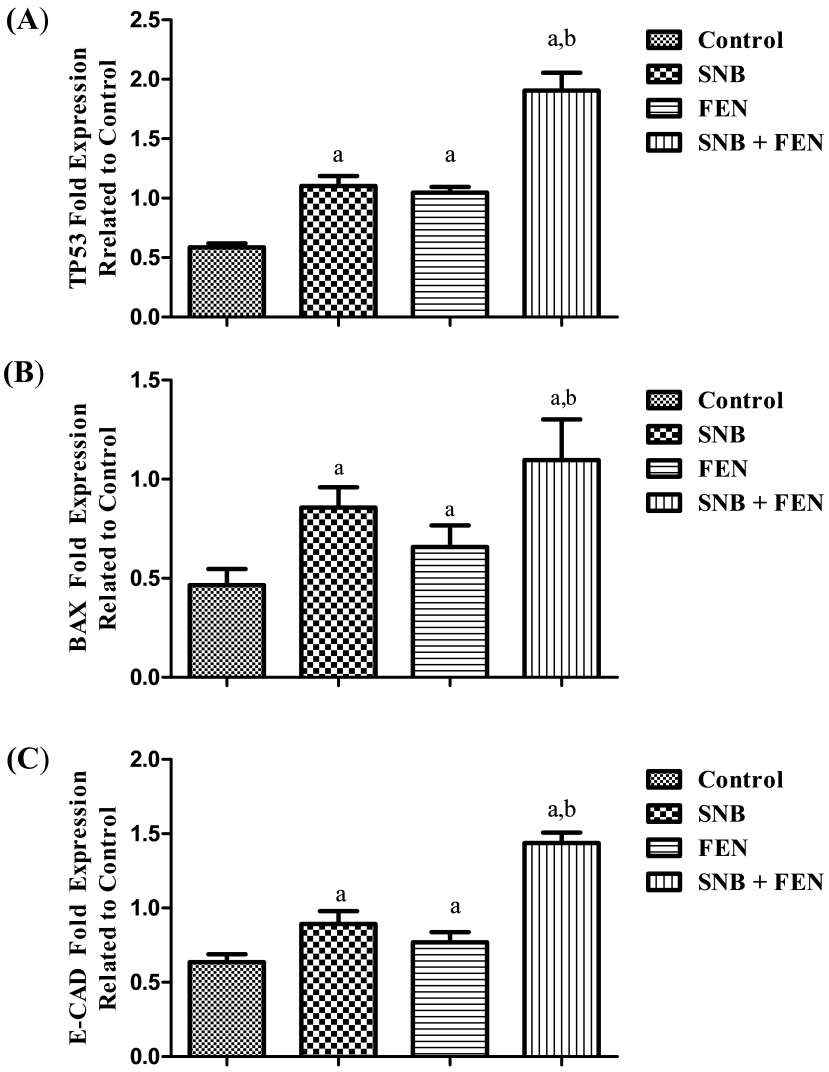


Fig. 4. Relative expression of *TP53*, *BAX*, and *CDH1* (*E-CAD*) in U87 cells following treatment with FEN and SNB. U87 cells were treated for 24 h with FEN (150 μM), SNB (100 nM), or their combination (FEN 150 μM + SNB 100 nM). Gene expression was determined by quantitative RT-PCR and normalized to *GAPDH*. *GAPDH* was used as the internal reference gene and assigned a relative expression value of 1 for normalization. The untreated control values represent the experimentally determined basal expression of each target gene relative to *GAPDH*. (**A**) *TP53*, (**B**) *BAX*, and (**C**) *CDH1* (*E-CAD*) expression. The data were expressed as the mean ± SD, 3 samples per group, letters a or b indicate the presence of a significant increase or decrease from the control group at $p \leq 0.05$.

DNMT inhibition may restore tumor suppressor gene expression and regulate proliferation and apoptosis. The superior binding profile of SNB highlights its greater potential for epigenetic modulation in GB therapy. See Fig. 6**A**, and 6**B**.

Both FFA and SNB bind favorably to the HDM catalytic pocket with comparable docking scores, –7.253 kcal/mol for FFA and –7.271 kcal/mol for SNB, suggesting similar inhibitory potential. FFA primarily interacts through coordination with the catalytic Fe^{2+} ion, disrupting demethylase activity. In contrast, SNB forms a broader interaction network, including hydrogen bonds and stronger metal coordination, enhancing binding stability. HDM inhibition may drive epigenetic remodeling and alter gene expression. SNB's extended interactions suggest more sustained inhibition and potential therapeutic benefit in GB. See Fig. 6**C** and 6**D**.

FFA and SNB show comparable binding to the IDH2 active site, with docking scores of –7.131 kcal/mol and –7.004 kcal/mol, respectively, and distinct but stable interaction modes involving key residues such as Arg119 and Tyr285, supporting their potential as IDH2 modulators. By targeting IDH2, both compounds may reduce 2-hydroxyglutarate accumulation and restore epigenetic balance. FFA primarily engages in aromatic interactions, while SNB forms strong polar contacts, suggesting comple-

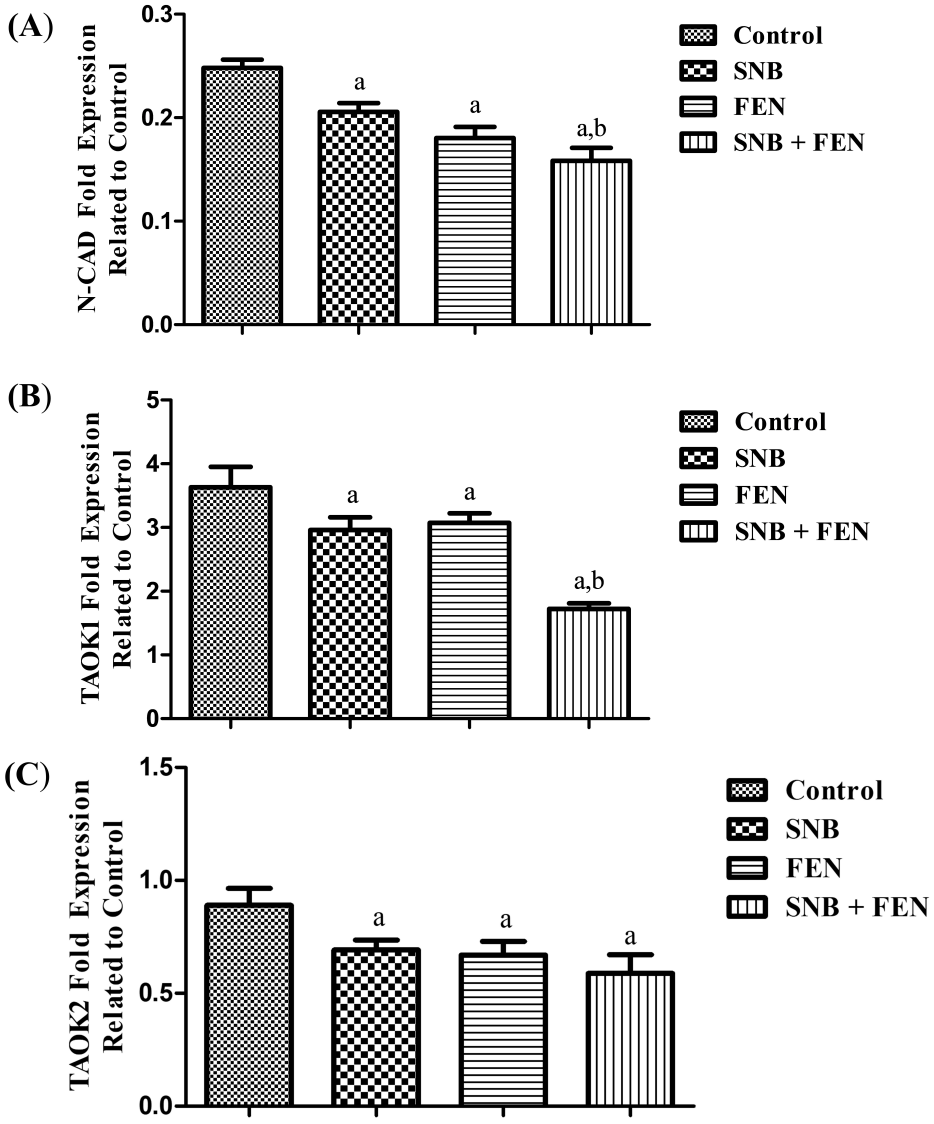


Fig. 5. Relative expression of *CDH2* (*N-CAD*), *TAOK1*, and *TAOK2* in U87 cells following treatment with FEN and SNB. U87 cells were treated for 24 h with FEN (150 μM), SNB (100 nM), or their combination (FEN 150 μM + SNB 100 nM). Gene expression was determined by quantitative RT-PCR and normalized to *GAPDH*. *GAPDH* was used as the internal reference gene and assigned a relative expression value of 1 for normalization. The untreated control values represent the experimentally determined basal expression of each target gene relative to GAPDH. (**A**) *CDH2* (*N-CAD*), (**B**) *TAOK1*, and (**C**) *TAOK2* expression. The data were expressed as the mean ± SD, 3 samples per group, letters a or b indicate the presence of a significant increase or decrease from the control group at $p \leq 0.05$.

mentary mechanisms of action. See Fig. 6**E** and 6**F**. Given the aggressive nature of GB, especially IDH-wildtype tumors, targeting metabolic pathways like IDH2 is promising. Their combined use may enhance therapeutic efficacy through significant inhibitory effect modulation of metabolic and signaling processes.

CDK4 is a key driver of GBM cell cycle progression (G1 → S phase), and its inhibition is a validated strategy to suppress tumor proliferation. In the present study, SNB gives the stronger binding affinity, with a docking score of –7.609 kcal/mol compared with –6.899 kcal/mol for FFA, and specific hydrogen bonds with Val96 and His95, indicating a more precise anchoring within the CDK4 active site. This suggests more effective inhibition of CDK4 activity, which could lead to cell cycle arrest, reduced tumor growth, and decreased proliferation of GBM cells. However, FFA participates in hydrophobic (π–H) interactions; the absence of stabilizing hydrogen bonds makes its binding less specific and potentially less effective at inhibiting CDK4. See Fig. 6**G** and 6**H**. Thus, SNB emerges as the more promising CDK4 inhibitor, with potential to better suppress GB cell proliferation, while FFA may have a weaker effect on

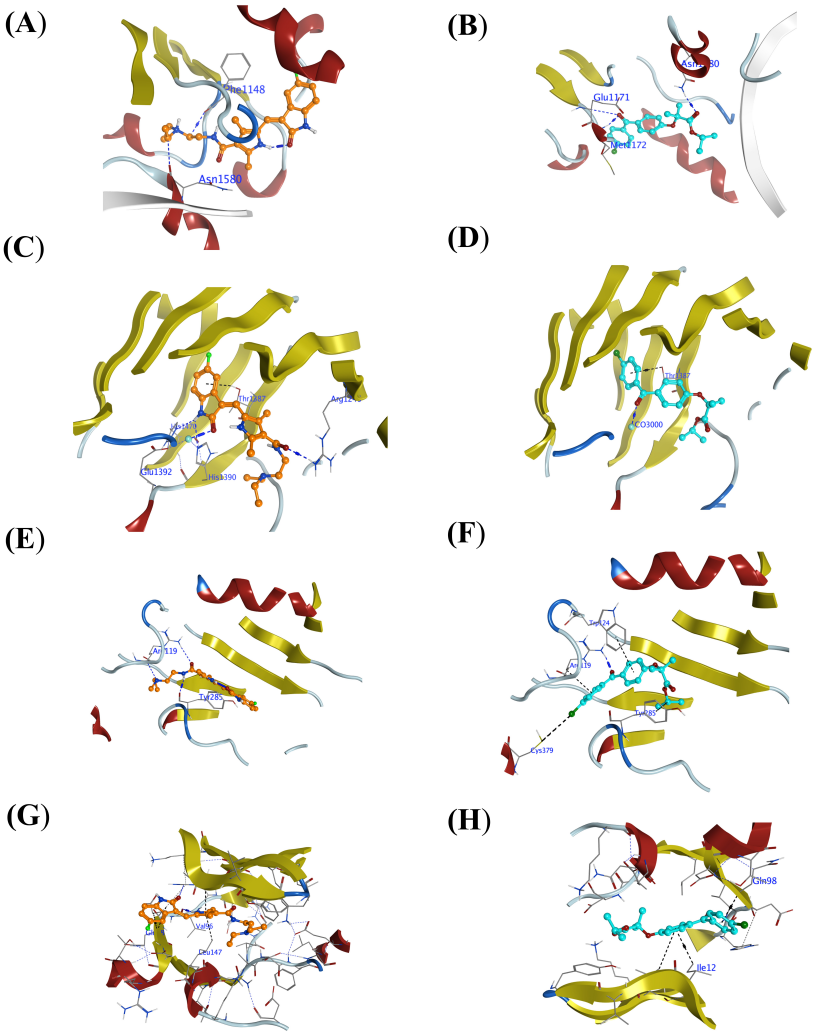


Fig. 6. Three-dimensional (3D) molecular docking poses of SNB (brown) and FFA (cyan) within the binding sites of DNMT (A–B), HDM (C–D), IDH2 (E–F), and CDK4 (G–H) illustrating their binding orientations and key noncovalent interactions, including hydrogen bonds, hydrophobic contacts, and electrostatic interactions.

cell cycle control.

Interaction of SNB and FFA With α-KGDH, SDH, SIT, and GLO-1

Docking shows both ligands bind α-KGDH, with SNB displaying slightly higher affinity and a more stable hydrophobic fit. As a key tricarboxylic acid (TCA) cycle enzyme, α-KGDH modulation disrupts mitochondrial redox balance, increasing reactive oxygen species (ROS) and promoting lipid peroxidation, a trigger of ferroptosis. SNB's stronger binding suggests greater potential to induce oxidative stress and ferroptotic cell death. Combined with GPX4 inhibition, this dual targeting may enhance therapeutic efficacy against resistant GB.

FFA and SNB showed favorable binding to KGDH. See Fig. 7**A** and 7**B**. The high binding affinity of SNB for SDH suggests a potential disruption of the metabolic pathway in GB. As SDH links the TCA cycle with the mitochondrial electron transport chain, its inhibition can alter succinate accumulation, promote HIF stabilization, and drive metabolic phenotypic restoration that supports tumor growth. Targeting SDH with FFA and SNB may impair metabolic plasticity, decreasing GB cell survival and proliferation, highlighting promise as modulators of vulnerabilities. See Fig. 7**C** and 7**D**.

Given the critical role of SIT in promoting GB progression, stemness, and immune evasion, inhibition of this enzyme represents a promising therapeutic strategy. Both ligands demonstrate favorable binding within the SIT catalytic cleft, supporting their potential as inhibitors relevant to GB therapy. However, FFA exhibits a slightly stronger binding affinity and a more extensive interaction network. This broader engagement suggests a more stable and effective occupation of the active site, which could translate into

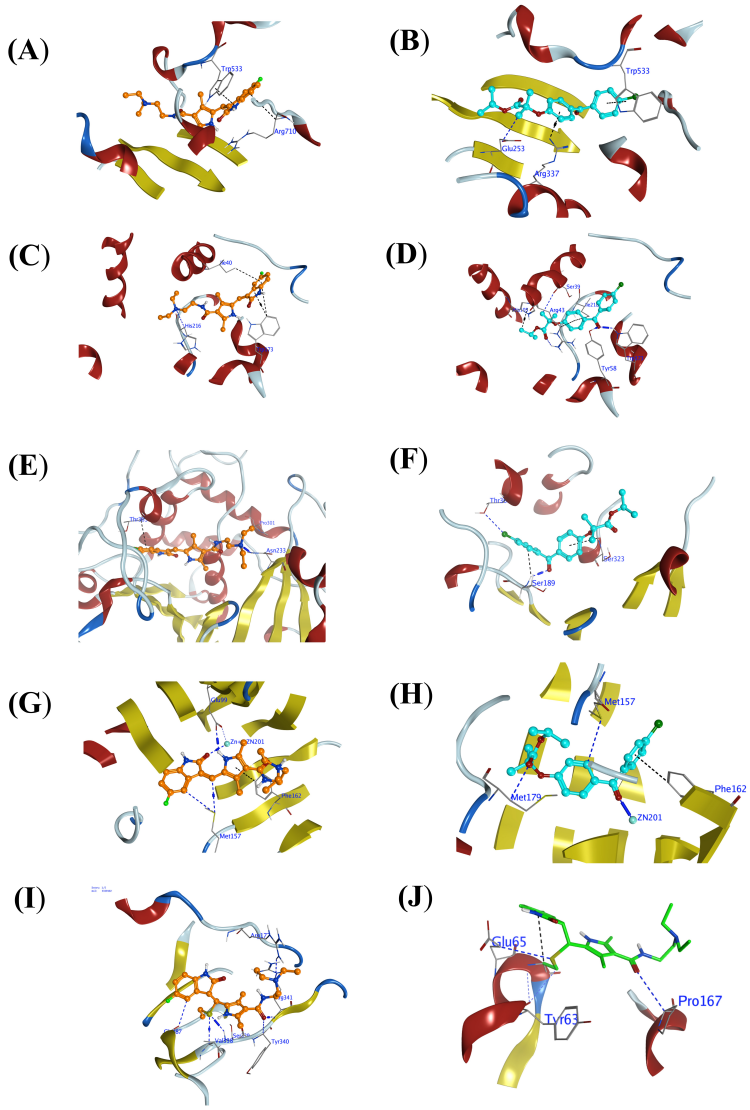


Fig. 7. Three-dimensional interaction profiles of SNB (brown) and FFA (cyan) with KGDH (A–B), SDH (C–D), SIT (E–F), GLO-1 (G–H), showing their binding orientations and key noncovalent interactions. Covalent docking of SNB with Caspase-8 (**I**) and GPX4 (**J**) illustrates the formation of stable covalent adducts at the reactive sites.

stronger inhibition of SIT activity. In contrast, SNB shows a more limited but targeted interaction profile. See Fig. 7**E** and 7**F**.

GLO-1 inhibition represents a promising GB strategy because the enzyme detoxifies MGO, enabling highly glycolytic tumor cells to tolerate metabolic stress. FFA showed stronger GLO-1 inhibition, likely promoting MGO accumulation, oxidative stress, and apoptosis, thereby suppressing proliferation. Although SNB binds less strongly, its hydrogen bonding and aromatic interactions suggest structural stability and selectivity, supporting its potential as a complementary scaffold for developing selective inhibitors targeting GBM metabolic vulnerabilities. See Fig. 7**G** and 7**H**.

Interaction of SNB and FFA With Caspase-8 and GPX4

SNB forms an irreversible C–S covalent adduct formed via Michael addition covalent bond with Cys285 of Caspase-8, with a covalent docking score of –6.661 kcal/mol, providing the primary interaction responsible for the predicted enzyme interaction. Following covalent attachment, SNB is stabilized by multiple noncovalent interactions within the active site, including hydrogen bonding with Gly287, Val338, Ser339, Tyr340, and Arg341, which position the ligand along the substrate-binding groove. The strong interaction with Ser339 contributes significantly to stabilizing the post-covalent complex, while Arg177 offers additional electrostatic support. Overall, FFA and SNB exhibit favorable binding, but through distinct interaction patterns reflecting their chemical characteristics. See Fig. 7 **I**.

Covalent docking indicates that SNB may interact

with GPX4 by forming a covalent C–S thioether bond formed through a Michael addition reaction with Cys66, with a covalent docking score of –4.431 kcal/mol. Since GPX4 suppresses ferroptosis, its inhibition promotes lipid peroxide accumulation and ferroptotic cell death in GB cells. Weak hydrogen-bond interactions with Tyr63, Glu65, and Pro167 stabilize SNB within the active site. This mechanism suggests SNB as a promising ferroptosis-inducing in aggressive GB. See Fig. 7**J**. Combined findings indicate that SNB and FFA complementarily target major GB survival pathways across CDK4, Caspase-8, GPX4, DNMT, Glyoxalase I, and histone demethylases. SNB mainly disrupts cell cycle control and irreversibly inhibits apoptotic and redox enzymes, while FFA primarily induces metabolic stress and epigenetic alterations through Glyoxalase I and HDM inhibition. Their combined effects impact oxidative stress, mitochondrial metabolism, and PCD, producing enhanced inhibitory effect cytotoxicity in U87 cells and highlighting a promising multi-target GBM therapeutic strategy. Table 3 indicates binding interactions and docking scores for FFA and SNB with HDM, DNMT, CDK4, GPX4, and CAS-8. As well, Table 4 shows: Binding interactions and docking scores for FFA and SNB with SIT, GLO-1, IDH2, α-KGDH, and SDH.

Discussion

GBM exhibits distinct genetic and clinical profiles, which resulted in poor prognoses [9]. The crosstalk among metabolic, genetic, and epigenetic programs contributes to the complexity of GBM therapy [1]. Moreover, protein glycation promotes glioma growth, invasion, and aggressiveness [10]. The formation of glycan coat on GBM plasma membranes [11] resulted in immune evasion, tumor invasion, and drug resistance [10]. Moreover, glycan coating helps GBM cells to escape PCD forms [10,30]. Targeting glyoxalase, SITs, and sialidases (neuraminidases) could be a potential therapeutic strategy for GBM [10,11].

Glioma remodeling offers promising GBM therapy by simultaneously targeting metabolism and oncogenic pathways. Drug combinations and repurposing can modulate multiple pathways including glucose/lipid metabolism, growth signaling, cell cycle, PCD, tumor suppressors, and growth factors. This study examined FEN's effects on GB phenotypic restoration using SNB as a reference anticancer. U87 cell viability, apoptosis, and cell-cycle were examined versus untreated controls. Expression of *TAOK1*, *TAOK2*, *CDH2*, *CDH1*, *TP53*, and *BAX* assessed oncogene/tumor-suppressor balance. Molecular docking predicted FEN and SNB interactions with GBM-relevant targets including DNMT, HDM, KGDH, IDH2, SDH, SIT, GLO-1, CDK4, Caspase-8, GPX4.

The findings of this study align with a wealth of research indicating that FEN, SNB, and their combination significantly induce mortality in U87 GB cells. SNB inhibits multiple receptor tyrosine kinases involved in GB progression and can exert cytotoxic effects on GB cells [31]. Therefore, SNB is used for the management of GBM and other cancers [23]. SNB can inhibit the phosphorylation of key signaling molecules, including Alpha serine- threonine kinase (AKT), MAPK, and Signal Transducer and Activator of Transcription-3 (STAT3), which are involved in GB cell survival [14]. TKI members have the potential for targeting glucose metabolism [32], thus SNB might suppress glucose uptake by cancer cells [33]. Herein, SNB has an additional benefit for remodeling cancer cell metabolism and improving patient outcomes [34]. Concurrently, FEN also exhibits considerable cytotoxic effects on U87 cells. However, FEN induces metabolic phenotypic restoration that leads to energy depletion in tumor cells. Furthermore, FEN inhibits survival cell signaling [18]. Moreover, FEN has been shown to inhibit tumor growth at the epigenetic level through suppressing DNA methyltransferase 1 (DNMT1) activity [35]. Therefore, FEN hinders the growth of tumor cells [36]. Importantly, FEN suppresses cell proliferation and EMT through its effect on *PPAR*-α [35].

It has been reported that *PPAR*-α agonists, including FEN, can suppress cancer cell growth via key signaling pathway inhibition of proliferation signals and modulate oncogenesis. Moreover, they inhibit glycolysis and promote fatty acid oxidation [36–38]. In this context, they inhibit glucose transport into cells, increase oxidative stress, and lessen ATP production [36–38]. As well, FEN can induce metabolic remodeling in cancer cells and enhance their sensitivity [36–38]. Thus, FEN influence tumor suppressor/oncogene balance [36–38]. These effects are based on cancer type; therefore, in GB cells, treatment with FEN induces chemosensitivity [36–38].

The existing apoptosis data are synchronized with a prior study that reported SNB multi-targeted kinase inhibition induces cancer cell death through mitochondrial dysfunction, oxidative stress, and activation of apoptosis cascades [39]. In addition, SNB targets glucose metabolism as an essential metabolite for cancer cells' growth [32]. Therefore, SNB used the treatment of several cancers, including GB [34]. However, GB cells exhibit pronounced overexpression of multidrug resistance (MDR), which is a key factor contributing to therapeutic failure and disease recurrence. [14]. Thus, combination therapy could resolve SNB therapeutic problems. Several studies indicated that FEN induces apoptosis [36–38]. These effects shift FEN from being a lipid-lowering agent to a compound that has cytotoxic properties. FEN could elicit antiproliferative and pro-apoptotic activities on GB cells with low systemic toxicity [40]. In this regard, FEN has been reported to promote apoptotic cell death in GB cells through modulation of apoptosis-related signaling pathways [40].

The present results of cell cycle are aligned with several studies that state the deregulation of the cell cycle-controlling pathway in GBM. Likewise, a previous study indicated that FEN induced cell cycle arrest and apopto-

Table 3. Binding interactions and docking scores for FFA and SNB with target proteins (HDM, DNMT, CDK4, GPX4, and CAS-8).

Target proteins	Ligand		Receptor	Interaction	Distance	E (kcal/mol)	Score (kcal/mol)
HDM	FFA	O 5	CO CO 3000 (A)	Metal	2.48	–1.2	–7.253
		6-ring	OG1 THR 1387 (A)	pi-H	3.91	–0.9	
	SNB	N 7	NE2 HIS 1390 (A)	H-donor	3.35	–0.4	–7.271
		N 7	NE2 HIS 1470 (A)	H-donor	3.85	–0.4	
		O 2	NH2 ARG 1246 (A)	H-acceptor	2.9	–0.8	
		O 3	CO CO 3000 (A)	Metal	2.41	–2.2	
		6-ring	OG1 THR 1387 (A)	pi-H	3.89	–0.3	
DNMT	FFA	O 4	ND2 ASN 1580 (A)	H-acceptor	3.31	–1.4	–6.838
		O 5	CA GLU 1171 (A)	H-acceptor	3.46	–0.4	
		O 5	N MET 1172 (A)	H-acceptor	3.04	–1	
	SNB	C 9	O PHE 1148 (A)	H-donor	2.95	–0.6	–8.242
		C 15	O ASN 1580 (A)	H-donor	3.06	–0.4	
CDK4	SNB	N 5	O VAL 96 (A)	H-donor	3.35	–1.6	–7.609
		O 3	CE1 HIS 95 (A)	H-acceptor	3.29	–0.4	
		5-ring	CD1 ILE 12 (A)	pi-H	3.6	–0.3	
		6-ring	CA GLN 98 (A)	pi-H	4.38	–0.8	
		5-ring	CA GLN 98 (A)	pi-H	3.96	–1	
	FFA	6-ring	CD1 ILE 12 (A)	pi-H	3.93	–0.6	–6.899
		6-ring	CA GLN 98 (A)	pi-H	3.63	–0.9	
GPX4	SNB covalent docking	S 8	CA TYR 63 (A)	H-acceptor	4.29	–0.5	–4.431
		S 8	CD1 TYR 63 (A)	H-acceptor	4.34	–0.3	
		S 8	CG GLU 65 (A)	H-acceptor	3.97	–0.3	
		O 10	CA PRO 167 (A)	H-acceptor	3.72	–0.5	
CAS-8	SNB covalent docking	C 35	O GLY 287 (A)	H-donor	3.26	–0.4	–6.661
		S 8	CA VAL 338 (B)	H-acceptor	3.52	–0.7	
		S 8	N SER 339 (B)	H-acceptor	3.63	–2.7	
		O 10	CA TYR 340 (B)	H-acceptor	3.28	–0.4	
		O 10	N ARG 341 (B)	H-acceptor	3.2	–1.1	
		N 12	NH1 ARG 177 (A)	H-acceptor	3.62	–0.3	

The table details ligand-receptor interactions, including interaction type, distance (Å), energy contribution (E, kcal/mol), and overall docking score (kcal/mol).

sis [18]. FEN treatment triggered cytotoxicity through cell cycle control in GB cells [40]. The pleiotropic effects of FEN on cell metabolism, growth, and death signaling determined cell cycle status in U87 cells [40]. In this context, FEN treatment results in the suppression of DNMT1 activity, reversal of cyclin-dependent kinase inhibitor 2A (*CDKN2A*) methylation, and restoration of *CDKN2A* expression [35]. Moreover, SNB activates proapoptotic mechanisms and regulates cell cycle [39]. These mechanisms induce cell cycle arrest via the *CDKN2A*/retinoblastoma protein (*RB*)/E2F Transcription Factor (E2F) transcription factor pathway. This supports the cytotoxic potential of FEN and its ability to remodeling U87 and attenuate their survival.

The relationship between *BAX* and *TP53* in GBM contributes to the tumor's violent behavior and resistance to therapies. *BAX* is often downregulated, while *TP53* is frequently deactivated, permitting GBM cells to escape apoptosis and promote unchecked cells proliferation and invasion [41]. This dysregulation accentuates the need for advanced therapeutic tactics targeting apoptotic pathways [41]. Addressing the *BAX* and *TP53* imbalance could lead to more effective interventions against this GBM malignant transformation [41].

The present results *TP53* and *BAX* genes expression are concurrent with several studies related to tumor suppressor genes with TKIs and *PPAR-*α agonists. In this context, TKIs can increase BAX expression by inhibiting EGFR, inducing cellular stress, and promoting apoptosis. Additionally, TKIs may restore *TP53* activity, enhancing apoptosis and sensitivity to treatments [42]. Similarly, *PPAR-*α agonists, such as FEN, can upregulate BAX and potentially influence *TP53* activation to promote cell death in GBM cells [43]. Activation of *PPAR-*α may also affect lipid metabolism and cell cycle regulation, thereby inducing apoptosis [43]. In this context, TKIs and *PPAR-*α agonists promote apoptosis and influence tumor progression [42,43].

Table 4. Binding interactions and docking scores for FFA and SNB with target proteins (SIT, GLO-1, IDH2, α-KGDH and SDH).

Target proteins	Ligand		Receptor	Interaction	Distance	E (kcal/mol)	Score (kcal/mol)
SIT	FFA	O 1	CA LEU 187 (A)	H-acceptor	3.53	–0.3	–7.04
		CL 1	OG1 THR 365 (A)	H-donor	3.36	–0.4	
		O 5	N SER 189 (A)	H-acceptor	2.98	–1.9	
		6-ring	N SER 189 (A)	pi-H	4.24	–0.4	
	SNB	N 4	ND2 ASN 233 (A)	H-acceptor	3.15	–2.6	–6.860
		6-ring	CA THR 365 (A)	pi-H	3.88	–0.4	
GLO-1	FFA	C 18	SD MET 157 (A)	H-donor	4.16	–0.3	–8.607
		O 4	CB MET 179 (A)	H-acceptor	3.08	–0.3	
		O 5	ZN ZN 201 (A)	Metal	2.12	–4.2	
		6-ring	CZ PHE 162 (A)	pi-H	4.46	–0.3	
	SNB	N 6	OE2 GLU 99 (B)	H-donor	3.24	–2.4	–7.7
		C 19	SD MET 157 (A)	H-donor	3.84	–0.7	
		C 27	SD MET 157 (A)	H-donor	4.09	–0.4	
		O 3	ZN ZN 201 (A)	Metal	2.79	–1	
		C 25	6-ring PHE 67 (B)	H-pi	4.59	–0.3	
		5-ring	CZ PHE 162 (A)	pi-H	4.29	–0.3	
IDH2	FFA	CL 1	SG CYS 379 (A)	H-donor	4.32	–0.6	–7.131
		O 5	NH1 ARG 119 (A)	H-acceptor	2.84	–2.1	
		C 10	6-ring TYR 285 (A)	H-pi	4.18	–0.5	
		6-ring	CG ARG 119 (A)	pi-H	3.86	–0.3	
		6-ring	6-ring TRP 124 (A)	pi-pi	4.35	–0.2	
	SNB	N 6	O TYR 285 (A)	H-donor	3.29	–2.1	–7.004
		O 2	NH1 ARG 119 (A)	H-acceptor	3.72	–0.4	
		N 4	CA ARG 119 (A)	H-acceptor	3.54	–0.5	
α-KGDH	FFA	C 7	OE2 GLU 253 (A)	H-donor	3.39	–0.3	–6.814
		6-ring	NH1 ARG 337 (A)	pi-cation	3.29	–0.6	
		6-ring	5-ring TRP 533 (A)	pi-pi	4.06		
	SNB	6-ring	CA ARG 710 (A)	pi-H	4.75	–0.3	–7.254
		5-ring	5-ring TRP 533 (A)	pi-pi	3.81	–0.1	
SDH	FFA	C 7	O SER 39 (C)	H-donor	3.3	–0.3	–7.824
		O 4	NH2 ARG 43 (C)	H-acceptor	3.25	–0.4	
		O 5	NE1 TRP 173 (B)	H-acceptor	2.83	–2.8	
		O 5	OH TYR 58 (D)	H-acceptor	2.88	–0.7	
		C 15	5-ring HIS 105 (C)	H-pi	3.94	–1.4	
		6-ring	CD1 ILE 218 (B)	pi-H	4.34	–0.3	
		6-ring	CD ARG 43 (C)	pi-H	3.94	–0.4	
	SNB	N 4	CB HIS 216 (B)	H-acceptor	3.64	–0.3	–7.964
		5-ring	CZ2 TRP 173 (B)	pi-H	3.78	–0.7	
		6-ring	CZ2 TRP 173 (B)	pi-H	4.81	–0.5	
		6-ring	CD1 ILE 40 (C)	pi-H	4.13	–0.3	

The table details ligand-receptor interactions, including interaction type, distance (Å), energy contribution (E, kcal/mol), and overall docking score (kcal/mol).

Additionally, the combination of TKIs and *PPAR*-α agonists can significantly affect apoptosis in GBM [42,43]. TKIs generally increased apoptosis in GBM [42]. Moreover, *PPAR*-α agonists can enhance pathway to promote apoptosis in GBM cells [42,43]. These mechanisms highlight the potential of combining FEN and SNB as therapeutic strategies for GBM control [42,43].

Overall, both TKIs and *PPAR*-α agonists significantly impact apoptotic pathways in GBM, suggesting that their combination may improve patient outcomes.

CDH1, a tumor suppressor gene primarily found in epithelial tissues, is crucial for maintaining cell-cell adhesion and tissue integrity [44]. Conversely, *CDH2*, classified as an oncogene, is predominantly expressed in neural and mesenchymal tissues [44]. The balance between *CDH1* and *CDH2* is critical for GBM behavior, with their expres-

sion shift contributing to tumor invasiveness and aggressive clinical outcomes [44].

The present findings are aligned with the former study that indicated the loss of *CDH1* expression correlates with increased tumor aggressiveness, metastasis, and enhanced cell motility in GB cells [44]. In this regard, restoring *CDH1* expression can inhibit GBM cell invasion and tumor growth [44]. On the contrary, *CDH2* overexpression in GBM facilitates EMT, promoting tumor progression, invasion, and resistance to PCD [44]. Thus, targeting the pathways that regulate *CDH1* and *CDH2* expression could lead to novel GBM treatment strategies.

The combination of *PPAR-*α agonists and TKIs offers significant inhibitory effect approach in GBM therapy via influencing *CDH1* and *CDH2* expression [45,46]. *PPAR-*α agonists, such as FEN, have shown potential anti-tumor effects and may influence cell viability and migration, although they have a direct impact on cadherins [45]. Similarly, TKIs target pathways involved in tumor proliferation and can affect cadherin expression through modulation of EMT-related pathways [47].

The effect of SNB and FEN on *CDH1* and *CDH2* in GBM suggested new mechanistic strategies and improve their therapeutic impact in GBM management.

Thousand and one amino acid kinases (TAOKs), including *TAOK1*, *TAOK2*, and *TAOK3*, are serine/threonine kinases that play critical roles in cancer biology [48,49]. These proteins localize to the cytoplasm and centrosomes during mitosis, suggesting shared mechanisms in regulating mitotic processes [48,49]. TAOKs interact with p38 MAPK in response to DNA damage, influencing microtubule dynamics and cell cycle regulation [48,49]. Despite the role of *TAOK1* and *TAOK2* in neurodevelopmental disorders, little information is available about their role in GBM [48,49].

The present results are synchronized with several studies that suggested the deregulation of *TAOKs* in cancer cells [48,49]. Dysregulation of *TAOK* genes was observed in several cancers, including GBM. Several studies suggested that targeting *TAOK* might reduce the tumor invasiveness of GBM [50]. Moreover, *TAOK2* participates in the DNA damage response and affects cancer cell movement by activating Rho family GTPases. Overexpression of *TAOK2* is associated with aggressive behaviors in cancer [48,49]. Targeting *TAOK1* and *TAOK2* may offer novel therapeutic strategies for GBM management.

It has been suggested that drug repurposing strategies targeting *TAOK* genes might be beneficial for cancer management [50]. However, *TAOKs* are members of the MAPK cascade; therefore, they participate in regulating cell proliferation, apoptosis, migration, and invasion [49]. Thus, they are playing an important role in tumorigenesis and progression. In this regard, *TAOK* kinases play a vital role in tumor cell signal transduction, cell cycle regulation, and the tumor microenvironment [49]. Hence, *TAOKs* are a potential target for cancer therapy [49], particularly in the context of TKI strategies; however, TKIs can interfere with the aberrant signaling pathways such as EGFR, which are commonly overexpressed in various types of human cancer [49,51]. Integrating TKIs and *TAOK* inhibition could potentially improve therapeutic efficacy. However, disrupting multiple signaling cascades is critical for GBM progression [49].

PPAR-α agonists can interact with various signaling pathways, including Janus kinase/signal transducer and activator of transcription (JAK/STAT), and MAPK [52]. Thus, *PPAR-*α agonists, with their capacity to regulate inflammatory gene expression and immune cell function while enhancing cellular antioxidant defenses, show promise as novel therapeutic interventions for neurological diseases [52]. FEN, a *PPAR-*α agonist, shows promise as an adjunct therapy in GB by phenotypic restoration lipid metabolism and modulating proliferation and survival pathways. It enhances the efficacy of TKIs, promotes apoptosis, and reduces inflammation. Targeting *TAOK1* and *TAOK2* alongside TKIs further disrupts key signaling cascades. The crucial inhibitory effect interplay among *PPAR-*α activation, *TAOK* inhibition, and TKIs represents a novel and promising therapeutic strategy for GBM.

GBM shows distinct expression patterns of IDH, a wild-type glioma that frequently presents in older patients and is characterized by aggressiveness and poor prognosis [9]. In contrast, IDH-mutant glioma is common in younger patients and often arises from lower-grade gliomas, typically leading to a better outcome [9]. IDH enzymes play a crucial role in maintaining cellular homeostasis by converting isocitrate into alpha-ketoglutarate [9]. However, mutations in IDH lead to the conversion of alpha-ketoglutarate into 2-hydroxyglutarate (2-HG) [9]. The accumulation of 2-HG causes methylation changes in DNA and histones, giving rise to unique metabolic and epigenetic features, as well as varying responses to treatments [9].

Docking results indicated that, FFA emerges as the more promising candidate due to its stronger binding and wider interaction coverage, while SNB may serve as a useful scaffold for further optimization toward selective inhibition. SIT is upregulated in high percentage of cancers [53]. Mostly, hypersialylation is involved in the progression, migration, and immune evasion of GBMs [10,11]. SIT adds sialic acid moieties that induce hypersialylation and abundant negative charges on cancer cell membranes [53]. Thus, targeting hypersialylation pathways presents a promising therapeutic avenue to improve cancer treatment outcomes [3]. For instance SIT inhibitors mitigate hypersialylation of cancer cells [54]. Additionally, combining hypersialylation-targeted therapies with immune checkpoint inhibitors holds promise for enhancing treatment outcomes in breast cancer [54]. Interestingly, a surplus of the negatively charged sialic acid present on the cell surface is potentially a cationic nanoparticle [3]. Thus, targeting hypersialylated breast cancer improves treatment effective-

ness and minimizes off-target effects [4,54]. It has been reported that the *PPAR*-α member can decrease sialic acid, alongside modulation of genes involved in glucose and lipid metabolism, which may influence sialylation [55].

MGO is a reactive dicarbonyl active compound that forms adducts with proteins, lipids, and DNA [10]. Specifically, MGO-protein interaction changes the cell signaling pathways that promote glioma cells' proliferation and survival [10]. In addition, protein glycation promotes glioma growth, invasion, and aggressiveness [10]. Thus, MGO is a potent tumorigenic agent and contributes to the development of glioma [10].

Collectively, *PPAR*-α is a member of a family of ligand-activated nuclear steroid hormone receptors that function as transcription factors [56,57]. Upon ligand binding, *PPAR*-α forms heterodimers with retinoid X receptors (RXR) and binds to specific DNA sequences to regulate the expression of target genes [56,57]. *PPAR*-α activation plays a critical role in glucose, lipid, and amino acid metabolism and regulates various physiological processes, including cell proliferation, apoptosis, inflammation, and oxidative stress [56,57]. The connection between *PPAR*-α and cancer was initially established when *PPAR*-α agonists were found to increase the incidence of liver tumors in rodent models [56,57]. However, this phenomenon was not replicated in humans, leading to *PPAR*-α not being recognized as an established molecular target for cancer therapy. More recent studies have reported reduced levels of *PPAR*-α in certain tumor types, while *PPAR*-α agonists have been shown to suppress tumor growth [56]. For instance, the *PPAR*-α agonist such as FEN induces cancer cells death [56,57]. Additionally, *PPAR*-α activation has been found to suppress the metastatic potential of melanoma both *in vitro* and *in vivo* [57]. It has been reported that *PPAR*-α expression was lower in high-grade gliomas, identifying it as an independent prognostic factor in GBM patients [56]. Notably, *PPAR*-α agonism or overexpression inhibited glioma cell proliferation, invasion, and aerobic glycolysis, ultimately suppressing glioma growth [56].

FEN has a pleiotropic effect and a favorable safety profile, positioning it as a potential therapeutic candidate for cancer management [19,58–60]. Beyond its lipid-lowering effects, FEN elicit anticancer activities through the regulation of redox balance, mitochondrial function, inflammation, and ferroptosis [19,58–60]. Moreover, FEN influences signaling pathways involved in these anticancer activities, including ROS, NF-κB, FoxO3A, ERK, and AMPK [19,58–60]. Emerging evidence suggests that FEN has modulatory effects on iron-driven ferroptotic cell death. Therefore, FEN elicits anticancer effects against several human cancer cell lines, including breast, liver, glioma, prostate, pancreas, and lung cancer cells [19,58–60]. In this context, FEN can inhibit cancer cell proliferation, induce apoptosis, cause cell-cycle arrest, and interfere with cancer cell invasion and migration [19,58–60]. Given its various beneficial properties, FEN is considered a promising candidate for repurposing as an anticancer drug in the treatment of various cancers [19,58–60].

Study limitations: Despite being the first study to comprehensively evaluate the combined anticancer effects of FEN and SNB against GB using cell viability, apoptosis, cell cycle analysis, gene expression profiling, and molecular docking, several limitations should be acknowledged. First, the study was conducted using only the U87 GB cell line, which limits the generalizability of the findings and does not fully capture the molecular and phenotypic heterogeneity of GBM. Future studies should validate the observed effects in additional GBM cell lines, including patient-derived and temozolomide-resistant models, as well as in appropriate *in vivo* models. Second, although apoptosis and cell-cycle progression were evaluated, more detailed time-dependent investigations would be valuable to better characterize the kinetics and sequence of cellular responses induced by FEN, SNB, and their combination. Extending the observation period and incorporating multiple time points could distinguish early apoptotic signaling from later-stage cell death and clarify whether cell-cycle arrest precedes apoptosis. Third, the molecular mechanisms suggested by the gene-expression and molecular-docking findings were not comprehensively validated at the protein level. Western blotting or other protein-based approaches should be employed in future studies to confirm changes in key proteins associated with apoptosis, cell-cycle regulation, EMT, and the proposed molecular targets, thereby strengthening the mechanistic interpretation of the findings. Finally, the present study did not directly investigate ferroptosis, despite the potential relevance of oxidative stress and GPX4-related signaling to GBM cell death. Future work should determine whether FEN/SNB treatment induces or modulates ferroptosis by assessing lipid peroxidation, intracellular iron levels, glutathione depletion, GPX4 and Solute Carrier Family 7 Member 11 (SLC7A11) expression, and the effects of ferroptosis-specific inhibitors or activators. Such investigations could provide further insight into whether ferroptosis contributes to the enhanced antitumor effect observed with the FEN/SNB combination.

Conclusions

In conclusion, this study demonstrates that FEN, particularly in combination with SNB, exerts promising anticancer effects against U87 GB cells. The combined treatment enhanced cytotoxicity and apoptosis, promoted G1-phase cell-cycle arrest, and favorably modulated the expression of key tumor suppressor, EMT-related, and oncogenic genes. Molecular docking further supported the potential interaction of FFA and SNB with multiple molecular targets implicated in GB progression. Collectively, these findings suggest that FEN may enhance the therapeutic activity of SNB through complementary mechanisms. However, further studies using additional GBM models, protein-level

validation, time-dependent mechanistic investigations, and assessment of ferroptosis are warranted to confirm these findings and clarify the underlying molecular mechanisms. Overall, the FEN/SNB combination represents a promising candidate for further preclinical investigation as a potential therapeutic strategy for GB.

List of Abbreviations

GBM, glioblastoma multiforme; FEN, fenofibrate; *PPAR-α*, peroxisome proliferator-activated receptor alpha; SNB, sunitinib; *TP53*, tumor protein 53; *BAX*, BCL2 associated X, apoptosis regulator; *CDH1*, epithelial cadherin; *CDH2*, neural cadherin; *TAOK1*, thousand and one kinase 1; *TAOK2*, thousand and one kinase 2; PCD, programmed cell death; EGFR, epidermal growth factor receptor; IDH, isocitrate dehydrogenase; MGO, methylglyoxal; TKI, tyrosine kinase inhibitor; ATP, adenosine triphosphate; RT-PCR, reverse transcription polymerase chain reaction; DNMT, DNA methyltransferase; HDM, histone demethylase; KGDH, α-ketoglutarate dehydrogenase; IDH2, isocitrate dehydrogenase-2; SDH, succinate dehydrogenase; SIT, sialyltransferase; GLO-1, glyoxalase-1; CDK4, cyclin-dependent kinase 4; GPX4, glutathione peroxidase-4; *GAPDH*, glyceraldehyde-3-phosphate dehydrogenase; FFA, fenofibric acid; Cys66, reactive cysteine residues; SD, standard deviation; EMT, epithelial–mesenchymal transition; TCA, tricarboxylic acid; MDR, multidrug resistance; *CDKN2A*, cyclin-dependent kinase inhibitor 2A; MAPK, mitogen-activated protein kinase; JAK, janus kinase/signal transducer; STAT, signal transducer and activator of transcription; RXR, retinoid X receptors; ROS, reactive oxygen species; GB, glioblastoma; MTT, 3-(4,5-dimethylthiazol-2-yl)-2,5-diphenyltetrazolium bro- mide; DMSO, dimethyl sulfoxide; PBS, phosphate buffer saline; RNase, Ribonuclease; MDB, Molecular Database; GBVI/WSA, Generalized Born Volume Integral/Weighted Surface Area free energy of binding; MOE, Molecular Operating Environment; AKT, Alpha serine-threonine kinase; STAT3, Signal Transducer and Activator of Transcription-3; SLC7A11, Solute Carrier Family 7 Member 11.

Availability of Data and Materials

All data generated or analyzed during this study are included in this published article.

Declaration of AI and AI-assisted Technologies in the Writing Process

During the preparation of this manuscript, ChatGPT was used to assist with grammatical and language corrections, improve syntax, and support the preparation of graphical illustrations. Following the use of this tool, the authors carefully reviewed and edited the content as necessary.

Author Contributions

SA, MA, HA, FA, MMA, and GIH contributed to the study's conception, design, data collection, and manuscript preparation. AHB and HHA conducted the molecular docking analysis. GIH contributed to the manuscript writing and editing. All the authors read, revised, and approved the final manuscript. All authors agree to take full responsibility for the accuracy, integrity, and final content of the published manuscript.

Ethics Approval and Consent to Participate

Not applicable.

Acknowledgments

Not applicable.

Funding

The authors extend their appreciation to the ongoing researcher funding program (ORF-2026-1037) at King Saud University, Riyadh, Saudi Arabia.

Conflict of Interest

The authors declare no conflicts of interest to report regarding the present study.

References

[1] Xu X, Peng Q, Jiang X, Tan S, Yang Y, Yang W, *et al*. Metabolic reprogramming and epigenetic modifications in cancer: from the impacts and mechanisms to the treatment potential. Experimental & Molecular Medicine. 2023; 55: 1357–1370. https://doi.org/10.1038/s12276-023-01020-1.

[2] Chen C, Liu J, Lin X, Xiang A, Ye Q, Guo J, *et al*. Crosstalk between cancer-associated fibroblasts and regulated cell death in tumors: insights into apoptosis, autophagy, ferroptosis, and pyroptosis. Cell Death Discovery. 2024; 10: 189. https://doi.org/10.1038/s41420-024-01958-9.

[3] Habeeb IF, Alao TE, Delgado D, Buffone Jr A. When a negative (charge) is not a positive: sialylation and its role in cancer mechanics and progression. Frontiers in Oncology. 2024; 14: 1487306. https://doi.org/10.3389/fonc.2024.1487306.

[4] Mereiter S, Jonsson G, Oliveira T, Helm J, Hoffmann D, Abeln M, *et al*. Tumor sialylation controls effective anti-cancer immunity in breast cancer. 2024. https://doi.org/10.1101/2023.09.20.558571.

[5] Cortes Ballen AI, Amosu M, Ravinder S, Chan J, Derin E, Slika H, *et al*. Metabolic reprogramming in glioblastoma multiforme: a review of pathways and therapeutic targets. Cells. 2024; 13: 1574. https://doi.org/10.3390/cells13181574.

[6] Obrador E, Moreno-Murciano P, Oriol-Caballo M, López-Blanch R, Pineda B, Gutiérrez-Arroyo JL, *et al*. Glioblastoma therapy: past, present and future. International Journal of Molecular Sciences. 2024; 25: 2529. https://doi.org/10.3390/ijms25052529.

[7] Zhuo S, He G, Chen T, Li X, Liang Y, Wu W, *et al*. Emerging role of ferroptosis in glioblastoma: Therapeutic opportunities and challenges. Frontiers in Molecular Biosciences. 2022; 9: 974156. https://doi.org/10.3389/fmolb.2022.974156.

[8] Grochans S, Cybulska AM, Simińska D, Korbecki J, Kojder K, Chlubek D, *et al*. Epidemiology of glioblastoma multiforme–literature review. Cancers. 2022; 14: 2412. https://doi.org/10.3390/cancers14102412.

[9] Fares J, Wan Y, Mair R, Price SJ. Molecular diversity in isocitrate dehydrogenase-wild-type glioblastoma. Brain Communications. 2024; 6: fcae108. https://doi.org/10.1093/braincomms/fcae108.

[10] Schildhauer P, Selke P, Staege MS, Harder A, Scheller C, Strauss C, *et al*. Glycation interferes with the expression of sialyltransferases and leads to increased polysialylation in glioblastoma cells. Cells. 2023; 12: 2758. https://doi.org/10.3390/cells12232758.

[11] Gargano D, Calvitto M, Niro A, Pepe G, Martella N, Tani A, *et al*. Sialylation Inhibition Impairs Migration and Promotes Adhesion of GBM Cells. International Journal of Molecular Sciences. 2025; 26: 10708. https://doi.org/10.3390/ijms262110708.

[12] Altwairgi AK, Algareeb W, Yahya G, Maklad AM, Aly MM, Al Shakweer W, *et al*. Outcome of patients with glioblastoma in Saudi Arabia: Single center experience. Molecular and Clinical Oncology. 2016; 4: 756–762. https://doi.org/10.3892/mco.2016.818.

[13] Tan AC, Ashley DM, López GY, Malinzak M, Friedman HS, Khasraw M. Management of glioblastoma: State of the art and future directions. CA: A Cancer Journal for Clinicians. 2020; 70: 299–312. https://doi.org/10.3322/caac.21613.

[14] Rahban M, Joushi S, Bashiri H, Saso L, Sheibani V. Characterization of prevalent tyrosine kinase inhibitors and their challenges in glioblastoma treatment. Frontiers in Chemistry. 2024; 11: 1325214. https://doi.org/10.3389/fchem.2023.1325214.

[15] Lyne SB, Yamini B. An alternative pipeline for glioblastoma therapeutics: a systematic review of drug repurposing in glioblastoma. Cancers. 2021; 13: 1953. https://doi.org/10.3390/cancers13081953.

[16] Abbruzzese C, Matteoni S, Signore M, Cardone L, Nath K, Glickson JD, *et al*. Drug repurposing for the treatment of glioblastoma multiforme. Journal of Experimental & Clinical Cancer Research. 2017; 36: 169. https://doi.org/10.1186/s13046-017-0642-x.

[17] Kounatidis D, Tentolouris N, Vallianou NG, Mourouzis I, Karampela I, Stratigou T, *et al*. The pleiotropic effects of lipid-modifying interventions: exploring traditional and emerging hypolipidemic therapies. Metabolites. 2024; 14: 388. https://doi.org/10.3390/metabo14070388.

[18] Basilotta R, Lanza M, Casili G, Chisari G, Munao S, Colarossi L, *et al*. Potential therapeutic effects of PPAR ligands in glioblastoma. Cells. 2022; 11: 621. https://doi.org/10.3390/cells11040621.

[19] Lian X, Wang G, Zhou H, Zheng Z, Fu Y, Cai L. Anticancer properties of fenofibrate: a repurposing use. Journal of Cancer. 2018; 9: 1527–1537. https://doi.org/10.7150/jca.24488.

[20] McKeage K, Keating GM. Fenofibrate: a review of its use in dyslipidaemia. Drugs. 2011; 71: 1917–1946. https://doi.org/10.2165/11208090-000000000-00000.

[21] Wilk A, Urbanska K, Grabacka M, Mullinax J, Marcinkiewicz C, Impastato D, *et al*. Fenofibrate-induced nuclear translocation of FoxO3A triggers Bim-mediated apoptosis in glioblastoma cells *in vitro*. Cell Cycle. 2012; 11: 2660–2671. https://doi.org/10.4161/cc.21015.

[22] Alobid S, Albassam H, Mirgany TO, Almutairi F, Alanazi MM, Bakheit AH, *et al*. Sunitinib and Fenofibrate as Combination Therapy for MDR Glioblastoma: Insights from *In Vitro* and *In Silico* Studies. Oncology Research. 2026; 34: 25. https://doi.org/10.32604/or.2025.073371.

[23] Alamón C, Dávila B, García MF, Sánchez C, Kovacs M, Trias E, *et al*. Sunitinib-containing carborane pharmacophore with the ability to inhibit tyrosine kinases receptors FLT3, KIT and PDGFR-β, exhibits powerful *in vivo* anti-glioblastoma activity. Cancers. 2020; 12: 3423. https://doi.org/10.3390/cancers12113423.

[24] Xiao X, Chen H, Yang L, Xie G, Shimuzu R, Murai A. Concise review: Cancer cell reprogramming and therapeutic implications. Translational Oncology. 2022; 24: 101503. https://doi.org/10.1016/j.tranon.2022.101503.

[25] Gong L, Yan Q, Zhang Y, Fang X, Liu B, Guan X. Cancer cell reprogramming: a promising therapy converting malignancy to benignity. Cancer Communications. 2019; 39: 48. https://doi.org/10.1186/s40880-019-0393-5.

[26] Saito S, Lin YC, Nakamura Y, Eckner R, Wuputra K, Kuo KK, *et al*. Potential application of cell reprogramming techniques for cancer research. Cellular and Molecular Life Sciences. 2019; 76: 45–65. https://doi.org/10.1007/s00018-018-2924-7.

[27] Saki S, TorabiParizi P. AI-Driven Approaches to Stem Cell Therapy in Cancer: Innovations and Challenges. International Journal of BioMed Insights. 2025; 2: 24–37. https://doi.org/10.22034/ijbmi.2025.222387.

[28] Majeed Y, Upadhyay R, Alhousseiny S, Taha T, Musthak A, Shaheen Y, *et al*. Potent and PPARα-independent anti-proliferative action of the hypolipidemic drug fenofibrate in VEGF-dependent angiosarcomas *in vitro*. Scientific Reports. 2019; 9: 6316. https://doi.org/10.1038/s41598-019-42838-y.

[29] Janssen JBE, Brahm CG, Driessen CML, Nuver J, Labots M, Kouwenhoven MCM, *et al*. The STELLAR trial: a phase II/III randomized trial of high-dose, intermittent sunitinib in patients with recurrent glioblastoma. Brain Communications. 2024; 6: fcae241. https://doi.org/10.1093/braincomms/fcae241.

[30] Shi J, Yang N, Han M, Qiu C. Emerging roles of ferroptosis in glioma. Frontiers in Oncology. 2022; 12: 993316. https://doi.org/10.3389/fonc.2022.993316.

[31] Ho KH, Lee YT, Chen PH, Shih CM, Cheng CH, Chen KC. Guanabenz Sensitizes Glioblastoma Cells to Sunitinib by Inhibiting GADD34-Mediated Autophagic Signaling. Neurotherapeutics. 2021; 18: 1371–1392. https://doi.org/10.1007/s13311-020-00961-z.

[32] S AK, Patel SS, Patel S, Parikh P. Future treatment of Diabetes–Tyrosine Kinase inhibitors. Journal of Diabetes & Metabolic Disorders. 2023; 22: 61–71. https://doi.org/10.1007/s40200-022-01164-3.

[33] Demirci A, Bal Ö, Durnali A, Ekinci AŞ, Eşbah O, Alkiş N, *et al*. Sunitinib-induced severe hypoglycemia in a diabetic patient. Journal of Oncology Pharmacy Practice. 2014; 20: 469–472. https://doi.org/10.1177/1078155213508441.

[34] Kong Y, Zhu HW, Tong HX, Shi L, Yu H. Proteome-wide and network pharmacology integration identifies sunitinib as a potential therapeutic for type 2 diabetes targets. Therapeutic Advances in Endocrinology and Metabolism. 2025; 16: 20420188251376325. https://doi.org/10.1177/20420188251376325.

[35] Kong R, Wang N, Han W, Bao W, Lu J. Fenofibrate exerts antitumor effects in colon cancer via regulation of DNMT1 and CDKN2A. PPAR Research. 2021; 2021: 6663782. https://doi.org/10.1155/2021/6663782.

[36] Chi T, Wang M, Wang X, Yang K, Xie F, Liao Z, *et al*. PPAR-γ modulators as current and potential cancer treatments. Frontiers in Oncology. 2021; 11: 737776. https://doi.org/10.3389/fonc.2021.737776.

[37] Sun J, Yu L, Qu X, Huang T. The role of peroxisome proliferator-activated receptors in the tumor microenvironment, tumor cell metabolism, and anticancer therapy. Frontiers in Pharmacology. 2023; 14: 1184794. https://doi.org/10.3389/fphar.2023.1184794.

[38] Tan Y, Wang M, Yang K, Chi T, Liao Z, Wei P. PPAR-α modulators as current and potential cancer treatments. Frontiers in Oncology. 2021; 11: 599995. https://doi.org/10.3389/fonc.2021.599995.

[39] Yang F, Jove V, Xin H, Hedvat M, Van Meter TE, Yu H. Sunitinib induces apoptosis and growth arrest of medulloblastoma tumor cells by inhibiting STAT3 and AKT signaling pathways. Molecular Cancer Research. 2010; 8: 35–45. https://doi.org/10.1158/1541-7786.mcr-09-0220.

[40] Giordano A, Macaluso M. Fenofibrate triggers apoptosis of glioblastoma cells *in vitro*: New insights for therapy. Cell Cycle. 2012; 11: 3154. https://doi.org/10.4161/cc.21719.

[41] Bai HL, Kang CM, Sun ZQ, Li XH, Dai XY, Huang RY, *et al*. TTDA inhibited apoptosis by regulating the p53-Bax/Bcl2 axis in glioma. Experimental Neurology. 2020; 331: 113380. https://doi.org/10.1016/j.expneurol.2020.113380.

[42] Frumento D, Grossi G, Falesiedi M, Musumeci F, Carbone A, Schenone S. Small molecule tyrosine kinase inhibitors (TKIs) for glioblastoma treatment. International Journal of Molecular Sciences. 2024; 25: 1398. https://doi.org/10.3390/ijms25031398.

[43] Ellis HP, Kurian KM. Biological rationale for the use of PPARγ agonists in glioblastoma. Frontiers in Oncology. 2014; 4: 52. https://doi.org/10.3389/fonc.2014.00052.

[44] Cao ZQ, Wang Z, Leng P. Aberrant N-cadherin expression in cancer. Biomedicine & Pharmacotherapy. 2019; 118: 109320. https://doi.org/10.1016/j.biopha.2019.109320.

[45] Annicotte JS, Iankova I, Miard S, Fritz V, Sarruf D, Abella A, *et al*. Peroxisome proliferator-activated receptor γ regulates E-cadherin expression and inhibits growth and invasion of prostate cancer. Molecular and Cellular Biology. 2006; 26: 7561–7574. https://doi.org/10.1128/mcb.00605-06.

[46] Osuka S, Zhu D, Zhang Z, Li C, Stackhouse CT, Sampetrean O, *et al*. N-cadherin upregulation mediates adaptive radioresistance in glioblastoma. The Journal of Clinical Investigation. 2021; 131: e36098. https://doi.org/10.1172/jci136098.

[47] Yang Y, Li S, Wang Y, Zhao Y, Li Q. Protein tyrosine kinase inhibitor resistance in malignant tumors: molecular mechanisms and future perspective. Signal Transduction and Targeted Therapy. 2022; 7: 329. https://doi.org/10.1038/s41392-022-01168-8.

[48] Elkhateeb N, Crookes R, Spiller M, Pavinato L, Palermo F, Brusco A, *et al*. Expanding the phenotype and genotype spectrum of TAOK1 neurodevelopmental disorder and delineating TAOK2 neurodevelopmental disorder. Genetics in Medicine. 2025; 27: 101348. https://doi.org/10.1016/j.gim.2024.101348.

[49] Li J, Wei X, Dong Z, Fu Y, Ma Y, Wu H. Research progress on antitumor mechanism of TAOK kinases. Cellular Signalling. 2024; 124: 111385. https://doi.org/10.1016/j.cellsig.2024.111385.

[50] Haddad N, Gamaethige SM, Wehida N, Elbediwy A. Drug repurposing: exploring potential anti-cancer strategies by targeting cancer signalling pathways. Biology. 2024; 13: 386. https://doi.org/10.3390/biology13060386.

[51] Tilak M, Holborn J, New LA, Lalonde J, Jones N. Receptor tyrosine kinase signaling and targeting in glioblastoma multiforme. International Journal of Molecular Sciences. 2021; 22: 1831. https://doi.org/10.3390/ijms22041831.

[52] Titus C, Hoque MT, Bendayan R. PPAR agonists for the treatment of neuroinflammatory diseases. Trends in Pharmacological Sciences. 2024; 45: 9–23. https://doi.org/10.1016/j.tips.2023.11.004.

[53] Nag S, Mandal A, Joshi A, Jain N, Srivastava RS, Singh S, *et al*. Sialyltransferases and Neuraminidases: Potential Targets for Cancer Treatment. Diseases. 2022; 10: 114. https://doi.org/10.3390/diseases10040114.

[54] Pietrobono S, Stecca B. Aberrant sialylation in cancer: biomarker and potential target for therapeutic intervention? Cancers. 2021; 13: 2014. https://doi.org/10.3390/cancers13092014.

[55] ur Rahman I, Idrees M, Salman M, Khan RU, Khan M, Amin F, *et al*. A comparison of the effect of glitazones on serum sialic acid in patients with type 2 diabetes. Diabetes & Vascular Disease Research. 2012; 9: 238–240. https://doi.org/10.1177/1479164111428629.

[56] Shi Y, Tao T, Liu N, Luan W, Qian J, Li R, *et al*. PPARα, a predictor of patient survival in glioma, inhibits cell growth through the E2F1/miR-19a feedback loop. Oncotarget. 2016; 7: 84623–84633. https://doi.org/10.18632/oncotarget.13170.

[57] Wang Y, Lei F, Lin Y, Han Y, Yang L, Tan H. Peroxisome proliferator-activated receptors as therapeutic target for cancer. Journal of Cellular and Molecular Medicine. 2024; 28: e17931. https://doi.org/10.1111/jcmm.17931.

[58] Mandala A, Armstrong A, Girresch B, Zhu J, Chilakala A, Chavalmane S, *et al*. Fenofibrate prevents iron induced activation of canonical Wnt/β-catenin and oxidative stress signaling in the retina. NPJ Aging and Mechanisms of Disease. 2020; 6: 12. https://doi.org/10.1038/s41514-020-00050-7.

[59] You BJ, Hour MJ, Chen LY, Luo SC, Hsu PH, Lee HZ. Fenofibrate induces human hepatoma Hep3B cells apoptosis and necroptosis through inhibition of thioesterase domain of fatty acid synthase. Scientific Reports. 2019; 9: 3306. https://doi.org/10.1038/s41598-019-39778-y.

[60] Dong X, Bin Y, Tong F, Kuang B. EP09.02-05 Fenofibrate enhances radiotherapy efficacy by elevating HDL levels to induce tumor cell ferroptosis in NSCLC with brain metastasis. Journal of Thoracic Oncology. 2023; 18: S597. https://doi.org/10.1016/j.jtho.2023.09.1125.

Editor's note: The Scientific Editors responsible for this paper were Xiaoyuan Ji and Martin Stoddart.

Received: 27th June 2026; **Accepted**: 21th September 2026; **Published**: 30th October 2026